On the Leading-Edge Suction and Stagnation Point Location in Unsteady Flows Past Thin Aerofoils

Kiran Ramesh[1]†

[1]Aerospace Sciences Division, School of Engineering, University of Glasgow, Glasgow, G12 8QQ, UK

(Received xx; revised xx; accepted xx)

Unsteady thin-aerofoil theory is a low-order method for calculating the forces and moment developed on a camber-line undergoing arbitrary motion, based on potential flow theory. The vorticity distribution is approximated by a Fourier series, with a special "A_0" term that is infinite at the leading edge representing the "suction peak". Though the integrated loads are finite, the pressure and velocity at the leading edge in this method are singular owing to the A_0 term. In this article, the principle of Matched Asymptotic Expansions (MAE) is used to resolve the singularity and obtain a uniformly valid first-order solution. This is performed by considering the unsteady thin-aerofoil theory as an outer solution, unsteady potential flow past a parabola as an inner solution, and by matching them in an intermediate region where both are asymptotically valid. Resolution of the leading-edge singularity allows for derivation of the velocity at the leading-edge and location of the stagnation point, which are of physical and theoretical interest. These quantities are seen to depend on only the A_0 term in the unsteady vorticity distribution, which may be interpreted as an "effective unsteady angle of attack". The leading-edge velocity is proportional to A_0 and inversely proportional to the square root of leading-edge radius, while the chord-wise stagnation point location is proportional to the square of A_0 and independent of the leading-edge radius. Closed-form expressions for these in simplified scenarios such as quasi-steady flow and small-amplitude harmonic oscillations are derived.

1. Introduction

Research in the fields of aeronautics and fluids dynamics is increasingly concerned with unsteady aerodynamics in the 21st century. Unsteady flow phenomena are present in a wide range of problems and in diverse fields. The study of biological high-lift flight based on flapping wings and large-scale vortex shedding, for example, is of interest to both biologists and engineers (Eldredge & Jones 2019). Unsteady flows exhibit rapid changes in circulation around the lifting surface, apparent-mass effects, flow separation and vortex shedding (Leishman 2002, chap. 8) .

Theoretical formulations and low-order models for unsteady flows are typically based on the Boundary-Element-Method (BEM) approach. These solve the unsteady potential flow equations with farfield boundary conditions being naturally enforced, and require calculations only on the modelled surface(s) and wake(s). Since unsteady flows involve changing circulation and shedding of vorticity from surfaces, inviscid vortex elements/sheets are used to model these phenomena (Darakananda & Eldredge 2019). The ease of setup/use and rapid solution times offered by these methods has made them widely useful for initial design and analysis. Panel methods are a type of BEM derived

† Email address for correspondence: kiran.ramesh@glasgow.ac.uk

by discretising the surface into geometric panels. Thin-aerofoil theory is derived from further simplifications where the aerofoil is assumed to be thin (consisting only of a camber-line), and the boundary condition is transferred from the camber line to the chord line. The vorticity distribution on the chord line is modelled by a general Fourier series, with a special "A_0" term that is infinite at the leading edge. This term represents the "suction peak" caused by the flow having to turn around the aerofoil leading edge when the stagnation point moves away from the leading edge. Despite the limiting assumptions in comparison with panel methods, thin-aerofoil theory has the advantage of providing closed-form expressions for forces and moment on the aerofoil, and physical interpretations for the Fourier coefficients. It may also be more accurate than panel methods for thin sections as it has no errors associated with geometric discretisation.

Originally developed for steady flows about an aerofoil at a constant angle of attack, thin-aerofoil theory has also been extended to unsteady flows (Katz & Plotkin 2000). Ramesh *et al.* (2013) have derived such a theory valid for arbitrarily large amplitudes and non-planar wakes. Though the need to model free vorticity interaction in the wake makes this method semi-numerical in comparison with completely closed-form theory like Theodorsen (1935), it is applicable to a wider range of scenarios occurring in nature and engineering. This method has been used in studies on diverse topics including design of efficient flapping aerofoils through morphing (Willis & Persson 2014), and power generation by self-sustained oscillation of an aeroelastic aerofoil (Ramesh *et al.* 2015). The "A_0" term in this method is of particular interest and has been used to develop a new aerodynamic entity called the Leading-Edge Suction Parameter (LESP) in Ramesh *et al.* (2014). It has been shown through experimental and numerical verification that the process of leading-edge vortex (LEV) formation is strongly correlated to the local suction at the leading edge and hence the LESP (Ramesh *et al.* 2018; Deparday & Mulleners 2018, 2019). This parameter has been used to predict and control the occurrence of LEV formation, and in discrete-vortex methods for modelling intermittent LEV shedding on aerofoils/wings where the LESP is used to both predict LEV formation and modulate the strength of discrete vortices shed from the leading edge (Ramesh *et al.* 2014, 2017; Hirato *et al.* 2019).

Despite these successful applications listed above, unsteady thin-aerofoil theory (UTAT) suffers from the defining limitation of having a singularity at the leading edge. Since the vorticity at this location is infinite, the pressure and velocity are also infinite. Forces and moments can still be obtained through integration of these quantities as the singularity is integrable. However, resolving the primitive variables near the leading edge is not only of academic interest, but also important for studying the properties of the boundary layer. The inviscid velocity/pressure over the aerofoil is also the edge velocity of the boundary layer and the unsteady boundary layer equations may be solved in field or integral form to predict events such as transition to turbulence and separation. In steady flows, this approach is used in the well known Stratford criterion for predicting flow separation (Stratford 1959) and in the design/analysis software XFOIL (Drela 1989), for example. The solution at the leading-edge also contains information about the stagnation point which is related to the circulatory effects and lift for an unsteady aerofoil, and has potential as a flow control parameter (Suryakumar *et al.* 2016; Saini & Gopalarathnam 2018).

In steady flows, the leading-edge singularity in thin-aerofoil theory was first resolved by Lighthill (1951) and later formalised by van Dyke (1964) through the method of Matched Asymptotic Expansions (MAE). In this approach, the exact potential-flow solution for the flow past a parabolic curve is "matched" with the thin-aerofoil solution that is singular at the leading edge, to produce a composite uniformly-valid solution.

MAE has been further developed by Rusak (1994) and Rusak (1993) for the subsonic and transonic flow regimes respectively, and by Morris & Rusak (2013) for the problem of leading-edge stall on thin aerofoils. James (1983) has used this method to resolve the singularity for a thin aerofoil undergoing small amplitude oscillations in pitch and heave, and having a planar wake (assumptions in Theodorsen (1935)). In this article, we apply the principle of MAE to obtain a uniformly-valid first-order solution for general unsteady thin-aerofoil theory which allows for arbitrarily large amplitudes and non-planar wakes. The theory is presented in sec. 2. The magnitude of flow velocity at the leading edge and location of the unsteady stagnation point which have important practical applications are derived in sec. 3, and closed-form expressions for these quantities in some simplified scenarios are presented.

2. Theory

The problem is formulated with two components: an "inner solution" (sec. 2.1) based on unsteady flow past a parabolic curve representing the leading edge, and an "outer solution" (sec. 2.2) derived from unsteady thin-aerofoil theory (which is singular at the leading edge). Composite solutions are derived by applying the principle of MAE in sec. 2.3.

2.1. *Inner Solution - unsteady flow past a parabola*

The inviscid inner solution is the flow about the rounded nose of a thin aerofoil which may be represented by a parabola. Similar to James (1983), the flow near the nose may be considered to be comprised of a stagnation-point point flow and a parallel (lifting) flow which results from the stagnation point moving away from the leading edge. The geometry is described in a coordinate system (x, y) with the parabola nose (leading edge) coinciding with the origin, and the parabola axis (chord direction) with the x-axis. This problem may be elegantly solved by conformal mapping to the complex plane, shown in figure 1

$$z = rc\left(\kappa - \frac{\kappa^2}{2}\right) \tag{2.1}$$

where $z = x + iy$, $\kappa = \epsilon + i\eta$ and r is the leading-edge radius nondimensionalised with respect to aerofoil chord. This transformation maps the flow field in the physical z plane to the left half of the κ-plane. The parabola $y = \pm\sqrt{2rcx}$ is mapped to the $\epsilon = 0$ line. The coordinates in the two planes are related as

$$y = rc\eta, \qquad x = rc\frac{\eta^2}{2} \tag{2.2}$$

For the stagnation-point flow, complex velocity in the κ-plane is

$$\vec{v} = U_s(-\epsilon + i\eta) \tag{2.3}$$

and the velocity potential and stream function are

$$\phi_s = U_s\frac{\eta^2 - \epsilon^2}{2}, \qquad \psi_s = -U_s\epsilon\eta \tag{2.4}$$

Similarly for the parallel flow,

$$\phi_p = U_p\eta, \qquad \psi_p = -U_p\epsilon \tag{2.5}$$

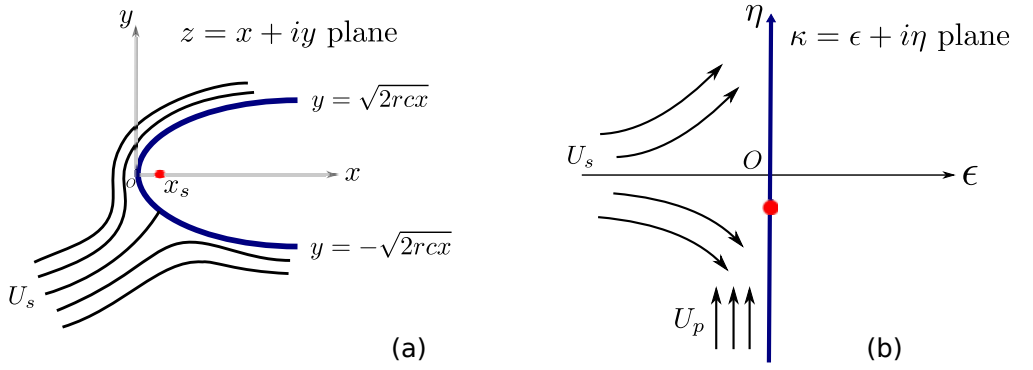

FIGURE 1. (a) Unsteady flow around a parabolic curve when the stagnation point has moved away from the leading edge, (b) transformed flow in the κ-plane decomposed as stagnation flow and parallel flow.

The total complex potential of the flow is given by

$$F = \phi + i\psi = \left(U_s \frac{\eta^2 - \epsilon^2}{2} + U_p \eta \right) - i \left(U_s \epsilon \eta + U_p \epsilon \right) \tag{2.6}$$

On the aerofoil surface given by $\epsilon = 0$, the complex potential

$$F = U_s \frac{\eta^2}{2} + U_p \eta \tag{2.7}$$

and turns out to be real and the same as the velocity potential.

The pressure difference across the parabola upper and lower surfaces is calculated from the unsteady Bernoulli equation

$$\frac{\Delta p(x)}{\rho} = \frac{p_l - p_u}{\rho} = \frac{1}{2}(q_u^2 - q_l^2) + \left(\frac{\partial \phi}{\partial t} \right)_u - \left(\frac{\partial \phi}{\partial t} \right)_l \tag{2.8}$$

where q_u and q_l are total flow velocities over the aerofoil upper and lower surfaces, evaluated from $|dF/dz|$.

From the complex velocity potential derived above in eqn. 2.6, using $\epsilon = 0$ for the aerofoil surface,

$$\frac{\partial \phi}{\partial t}_{(\epsilon=0)} = \frac{\dot{U}_s}{2} \eta^2 + \dot{U}_p \eta \tag{2.9}$$

$$\left| \frac{dF}{dz} \right|_{(\epsilon=0)} = \frac{U_p + U_s \eta}{rc\sqrt{1+\eta^2}} \tag{2.10}$$

In the z-plane, $\eta = \pm\sqrt{2x/rc}$ on the aerofoil upper and lower surface, and

$$\frac{\partial \phi}{\partial t}_{u/l} = \dot{U}_s \frac{x}{rc} \pm \dot{U}_p \sqrt{\frac{2x}{rc}} \tag{2.11}$$

Expressing velocities as positive going from leading edge to trailing edge on both upper and lower surfaces of the aerofoil,

$$q_{u/l} = \pm \left| \frac{dF}{dz} \right|_{(\epsilon=0)} = \frac{U_s \sqrt{2x} \pm U_p \sqrt{rc}}{rc\sqrt{2x + rc}} \tag{2.12}$$

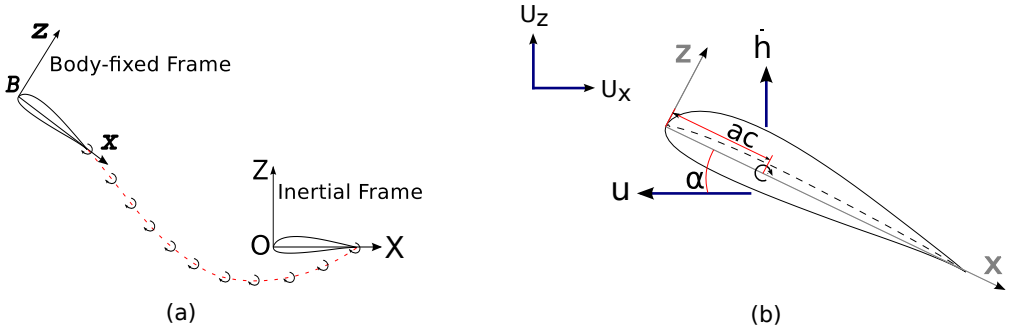

FIGURE 2. (a) Illustration of unsteady thin-aerofoil theory and the time-stepping method, (b) aerofoil and external velocities (positive as shown) and pitch-axis location.

The pressure difference variation over the parabola is

$$\frac{\Delta p(x)}{\rho} = \frac{2\sqrt{2x}U_s U_p}{rc\sqrt{rc}(2x+rc)} + 2\dot{U}_p\sqrt{\frac{2x}{rc}} \tag{2.13}$$

2.2. *Outer solution - unsteady thin-aerofoil theory*

The inviscid outer solution is from an unsteady thin-aerofoil formulation based on a time-stepping approach. The method is valid for arbitrary variations in freestream velocity and aerofoil kinematics, and contains no assumptions of small motion amplitudes or planar wakes (which are necessary in fully closed-form theories). Figure 2(a) illustrates the method, with the inertial reference frame given by $OXYZ$ and the body frame (attached to the moving aerofoil) by $Bxyz$. The two frames coincide at time $t = 0$ and at each time step, a discrete trailing-edge vortex (TEV) is shed from the trailing-edge.

The vorticity distribution over the aerofoil $\gamma(x)$ is taken as a Fourier series,

$$\gamma(\theta, t) = 2U_{ref}\left[A_0(t)\frac{1+\cos\theta}{\sin\theta} + \sum_{n=1}^{\infty} A_n(t)\sin(n\theta)\right] \tag{2.14}$$

where θ is a variable of transformation related to the chord-wise coordinate as

$$x = \frac{c}{2}(1-\cos\theta) \tag{2.15}$$

and $A_0(t)$, $A_1(t)$, ..., $A_n(t)$ are time-dependent Fourier coefficients, c is the aerofoil chord, and U_{ref} is a reference velocity for nondimensionalisation chosen according to the problem. The Kutta condition (zero vorticity at the trailing-edge) is enforced implicitly through the form of the Fourier series. The Fourier coefficients are determined from the instantaneous local downwash, $W(x,t)$, by enforcing the zero-normal-flow boundary condition on the aerofoil camber line,

$$A_0(t) = -\frac{1}{\pi}\int_0^{\pi}\frac{W(x,t)}{U_{ref}}d\theta, \qquad A_n(t) = \frac{2}{\pi}\int_0^{\pi}\frac{W(x,t)}{U_{ref}}\cos n\theta d\theta. \tag{2.16}$$

The normal downwash on the aerofoil camber line transferred to the chord line is determined from the aerofoil and freestream velocities shown in figure 2(b)

$$W(x,t) = \frac{\partial \eta_c}{\partial x}\left((U_X+u)\cos\alpha + (\dot{h}-U_Z)\sin\alpha + \frac{\partial \phi_w}{\partial x}\right) - (U_X+u)\sin\alpha - \dot{\alpha}(x-ac) + (\dot{h}-U_Z)\cos\alpha - \frac{\partial \phi_w}{\partial z} \quad (2.17)$$

where $\eta_c(x)$ is the camber variation on the aerofoil, a is the nondimensional location of the pitch axis from $0--1$, and $\frac{\partial \phi_w}{\partial x}$ and $\frac{\partial \phi_w}{\partial z}$ are velocities induced on the camber-line in directions tangential and normal to chord by discrete vortices in the wake. Arbitrary motion kinematics of the aerofoil in the 2D plane are represented by the time-varying parameters - plunge velocity in the Z direction $\dot{h}(t)$, horizontal velocity in the $-X$ direction $u(t)$, and pitch angle $\alpha(t)$. The velocities $U_X(t)$ and $U_Z(t)$ are horizontal and vertical components of external flow which may also result from gusts or other perturbations. The strengths of trailing-edge vortices (TEVs) shed at every time-step are solved for such that Kelvin's circulation condition is enforced.

$$\Gamma_B(t) + \sum \Gamma_{TEVs} = 0 \quad (2.18)$$

where Γ_B is the bound circulation, calculated by integrating the vorticity distribution (eqn. 2.14) over the aerofoil chord.

$$\Gamma_B(t) = U_{ref} c\pi \left(A_0(t) + \frac{A_1(t)}{2}\right) \quad (2.19)$$

Detailed description of this approach and its implementation may be found in Ramesh *et al.* (2013) and Ramesh *et al.* (2014). For further discussion in this article, we assume that the aerofoil travels at a constant horizontal velocity and that there are no external disturbances. The reference velocity is taken as the horizontal velocity.

$$u(t) = U_{ref} = u, \qquad U_X = U_Z = 0 \quad (2.20)$$

The variation of pressure difference between the upper and lower surfaces over the aerofoil ($\Delta p = p_l - p_u$) is again derived from the unsteady Bernoulli equation (eqn. 2.8) as

$$\frac{\Delta p(x)}{\rho} = \left(u\cos\alpha + \dot{h}\sin\alpha + \frac{\partial \phi_w}{\partial x}\right)\gamma(x) + \frac{\partial}{\partial t}\int_0^x \gamma(x)dx \quad (2.21)$$

where the second term may be evaluated from eqn. 2.14 as

$$\frac{\partial}{\partial t}\int_0^x \gamma(x)dx = uc\left(\dot{A}_0(\theta+\sin\theta) + \dot{A}_1\left(\frac{\theta}{2} - \frac{\sin 2\theta}{4}\right)\right) + uc\sum_{2,3,\ldots n}\frac{\dot{A}_n}{2}\left(\frac{\sin(n-1)\theta}{n-1} - \frac{\sin(n+1)\theta}{n+1}\right) \quad (2.22)$$

2.3. *Asymptotic matching and uniformly-valid solution*

Asymptotic matching of the inner and outer solutions is performed by equating them in an intermediate region where both are asymptotically valid. In this region, the value of the chord-wise coordinate x is small for the outer solution and large for the inner solution.

Taking the limit as x and θ tending to zero in the outer solution (eqn. 2.21) and expressing the result in x,

$$\frac{\Delta p(x)}{\rho} = 2uA_0\sqrt{\frac{c}{x}}\left(u\cos\alpha + \dot{h}\sin\alpha + \frac{\partial\phi_w}{\partial x}\right) + 4u\dot{A}_0\sqrt{cx} \tag{2.23}$$

Taking the limit as x tends to infinity in the inner solution (eqn. 2.13),

$$\frac{\Delta p(x)}{\rho} = \frac{\sqrt{2}U_sU_p}{rc\sqrt{rcx}} + 2\dot{U}_p\sqrt{\frac{2x}{rc}} \tag{2.24}$$

Equating the expressions for pressure difference in the intermediate region from the inner and outer solutions, we obtain expressions for the stagnation flow and parallel flow velocities in terms of unsteady thin-aerofoil theory variables.

$$U_s = rc\left(u\cos\alpha + \dot{h}\sin\alpha + \frac{\partial\phi_w}{\partial x}\right), \qquad U_p = \sqrt{2r}ucA_0 \tag{2.25}$$

Hence the exact solutions for pressure difference and velocity near the aerofoil leading edge (derived from the parabola) are

$$\frac{\Delta p(x)}{\rho} = \frac{8u\sqrt{cx}A_0}{rc+2x}\left(u\cos\alpha + \dot{h}\sin\alpha + \frac{\partial\phi_w}{\partial x}\right) + 4u\sqrt{cx}\dot{A}_0 \tag{2.26}$$

$$q = \frac{\sqrt{x}\left(u\cos\alpha + \dot{h}\sin\alpha + \frac{\partial\phi_w}{\partial x}\right) \pm \sqrt{c}uA_0}{\sqrt{x+\frac{rc}{2}}} \tag{2.27}$$

We note that these expressions are not singular at the leading edge, and that the values of pressure and velocity at the leading edge are associated with only the first Fourier term, A_0.

A uniformly-valid composite solution for pressure difference across the unsteady aerofoil is obtained from van Dyke's principle of MAE as : "outer solution (eqn. 2.21)" + "inner solution (eqn. 2.13)" - "common part (eqn. 2.24 or 2.23)".

$$\begin{aligned}\frac{\Delta p}{\rho} = {} & 2u\left(u\cos\alpha + \dot{h}\sin\alpha + \frac{\partial\phi_w}{\partial x}\right) \\ & \left[A_0\left(\frac{4c\sin(\theta/2)}{rc+2c\sin^2(\theta/2)} - \tan(\theta/4)\right) + \sum_{1,2,\ldots n} A_n\sin n\theta\right] \\ & + uc\left[\dot{A}_0(\theta+\sin\theta) + \dot{A}_1\left(\frac{\theta}{2} - \frac{\sin 2\theta}{4}\right) + \sum_{2,3,\ldots n}\frac{\dot{A}_n}{2}\left(\frac{\sin(n-1)\theta}{n-1} - \frac{\sin(n+1)\theta}{n+1}\right)\right]\end{aligned} \tag{2.28}$$

Following the same procedure as for pressure difference, a uniformly valid solution for the tangential velocity q can be derived as

$$q_{u/l} = \mp uA_0 \tan(\theta/4) \pm u \sum_{1,2,\ldots n} A_n \sin n\theta + \sqrt{\frac{x}{x+\frac{rc}{2}}} \left(u\cos\alpha + \dot{h}\sin\alpha + \frac{\partial \phi_w}{\partial x} \pm uA_0 \sqrt{\frac{c}{x}} \right) \quad (2.29)$$

The forces and pitching moment on the aerofoil, obtained by integrating the pressure difference eqn. 2.28 are unchanged from those obtained from the singular expression eqn. 2.21. The solution for the unsteady thin-aerofoil problem is still of first order, but now uniformly valid with no singularities in the primitive variables.

3. Results and Validation

3.1. *Velocity at leading edge and location of stagnation point*

The velocity in the vicinity of an unsteady aerofoil's leading edge is given by eqn. 2.27. This expression is seen to have a similar form to that derived for steady flow (van Dyke 1956), with A_0 replacing a parameter that is related to the steady angle of attack. This is consistent with the fact that in previous research (Ramesh *et al.* 2013, 2014), the A_0 term in unsteady thin-aerofoil theory has been shown to be an "effective unsteady angle of attack" consisting of contributions from the geometric angle of attack, aerofoil camber, plunge velocity and induced velocities by the wake.

The velocity at the unsteady aerofoil's leading edge is derived from eqn. 2.27 (or 2.29)

$$q_{LE} = \sqrt{\frac{2}{r}} uA_0 \quad (3.1)$$

The leading-edge velocity being proportional to A_0 is well established in unsteady thin-aerofoil theory and has previously been derived through a limit process applied at the leading edge. From Garrick (1937) and von Kármán & Burgers (1963), the form of the theoretically infinite velocity is given by

$$q_{LE} = \lim_{x\to 0} \frac{S}{\sqrt{x}} \quad (3.2)$$

where S is a measure of leading-edge suction

$$S = \lim_{x\to 0} \frac{1}{2}\gamma(x,t)\sqrt{x} \quad (3.3)$$

which is finite and proportional to A_0 (Ramesh *et al.* 2014) when evaluated using the current thin-aerofoil formulation. This was the theoretical basis for defining the Leading Edge Suction Parameter (LESP) equal to A_0 in Ramesh *et al.* (2014). Asymptotic matching in this article provides a finite value of the leading-edge velocity and further reveals that it is inversely proportional to square root of the aerofoil leading-edge radius.

The location of the stagnation point may be determined by applying the condition $q = 0$. The sign of A_0 indicates the stagnation point as lying on the lower surface (if positive) or on the upper surface (if negative). If the value of A_0 (effective unsteady angle of attack) is small, the stagnation point is close to the leading edge and well approximated by a simple expression from the parabola solution eqn. 2.27.

$$\sqrt{\frac{x_s}{c}} = \frac{u}{u\cos\alpha + \dot{h}\sin\alpha + \frac{\partial\phi_w}{\partial x}} A_0 \tag{3.4}$$

Closed-form expressions for the leading edge velocity and stagnation point in some simplified scenarios may be derived from eqns. 3.1 and 3.4.

3.1.1. *Steady aerofoil*

Considering steady flow around a thin aerofoil without camber at constant angle of attack,

$$\eta_c = 0, \qquad \dot{h} = 0, \qquad \frac{\partial\phi_w}{\partial x} = \frac{\partial\phi_w}{\partial z} = 0 \tag{3.5}$$

$$A_0 = \sin\alpha \tag{3.6}$$

$$q_{LE} = \sqrt{\frac{2}{r}} u \sin\alpha \tag{3.7}$$

$$x_s = c\tan^2\alpha \tag{3.8}$$

3.1.2. *Quasi-steady theory of unsteady aerofoil*

Considering an unsteady aerofoil without camber and applying the quasi-steady assumption (induced velocities by wake are neglected),

$$\eta_c = 0, \qquad \frac{\partial\phi_w}{\partial x} = \frac{\partial\phi_w}{\partial z} = 0 \tag{3.9}$$

$$A_0 = \sin\alpha - \frac{\dot{h}}{u}\cos\alpha + \frac{\dot{\alpha}c}{u}\left(\frac{1}{2} - a\right) \tag{3.10}$$

$$q_{LE} = \sqrt{\frac{2}{r}}\left(u\sin\alpha - \dot{h}\cos\alpha + \dot{\alpha}c\left(\frac{1}{2} - a\right)\right) \tag{3.11}$$

$$x_s = c\left(\frac{u\sin\alpha - \dot{h}\cos\alpha + \dot{\alpha}c\left(\frac{1}{2} - a\right)}{u\cos\alpha + \dot{h}\sin\alpha}\right)^2 \tag{3.12}$$

3.1.3. *Theodorsen's theory of unsteady aerofoil*

In Theodorsen (1935), an unsteady aerofoil without camber undergoes small harmonic oscillations in pitch and plunge at a reduced frequency $k = \omega c/2u$, and small-angle simplifications are applied ($\sin\alpha \approx \alpha$, $\cos\alpha \approx 1$). The wake is assumed to be planar and extending to infinity, on the basis of which closed-form expressions are derived for the velocities induced by the wake on the aerofoil. The vorticity distribution on the aerofoil in Theodorsen's theory is derived in Epps & Roesler (2018). The vorticity is partitioned into a non-circulatory part γ_n, a circulatory part associated with the motion γ_{c0} (the quasi-steady part), and a circulatory part associated with the wake γ_w.

Expressing these vorticity components from Epps & Roesler (2018) in terms of the chord-wise transformation variable θ, we have

$$\gamma_n = \frac{2}{\sin\theta}\left(W_{3qc}\cos\theta - \frac{\dot{\alpha}c}{4}(\cos\theta + \cos 2\theta)\right) \tag{3.13}$$

$$\gamma_{c0} = \frac{2W_{3qc}}{\sin\theta} \tag{3.14}$$

$$\gamma_w = -2ikW_{3qc}S(k)\left(Q_0(k)\frac{1+\cos\theta}{\sin\theta} + \sum_{n=1}^{\infty} Q_n(k)\sin n\theta\right) \tag{3.15}$$

where W_{3qc} is the normal downwash at the aerofoil three-quarter chord location,

$$W_{3qc} = u\alpha - \dot{h} - \dot{\alpha}c\left(a - \frac{3}{4}\right) \tag{3.16}$$

S(k) is the Sears function

$$S(k) = \frac{1/ik}{K_1(ik) + K_0(ik)} \tag{3.17}$$

and the wake coefficients are defined as

$$Q_n(k) = \int_0^{\infty} e^{-ik\cosh\zeta} e^{-n\zeta} d\zeta \tag{3.18}$$

The first two wake coefficients may be evaluated analytically (Epps & Roesler 2018) as

$$Q_0 = K_0(ik), \qquad Q_1(k) = K_1(ik) - \frac{1}{ik}e^{-ik} \tag{3.19}$$

while the remaining terms must be calculated numerically. In the equations above, $K_n(ik)$ is the modified Bessel function of the second kind of order n.

Equating the vorticity formulation in unsteady thin-aerofoil theory (eqn. 2.14) with these expressions, the equivalent Fourier coefficients are derived as

$$\begin{aligned} A_0 &= C(k)\frac{W_{3qc}}{u} - \frac{\dot{\alpha}c}{4u} \\ A_1 &= \frac{\dot{\alpha}c}{2u} - 2\frac{W_{3qc}}{u}(C(k) - e^{-ik}S(k)) \\ A_{2\ldots n} &= (-1)^n 2ikS(k)\frac{W_{3qc}}{u}Q_n \end{aligned} \tag{3.20}$$

where $C(k)$ is Theodorsen's function, a complex number dependent on reduced frequency. This function models the induced velocity of the wake, and effects an amplitude reduction and phase shift.

$$C(k) = \frac{K_1(ik)}{K_1(ik) + K_0(ik)} \tag{3.21}$$

The Fourier coefficients corresponding to Theodorsen's theory may also be directly derived from UTAT eqns. 2.16 and 2.17 by applying small-angle approximations, equating chord-wise wake induced velocity $\partial\phi_w/\partial x$ to zero (due to planar wake assumption) and calculating the chord-normal wake induced velocity from the thin-aerofoil result Katz & Plotkin (2000),

$$\frac{\partial \phi_w}{\partial z} = \frac{1}{2\pi} \int_0^\pi \gamma_w \frac{\sin\theta_0 d\theta_0}{\cos\theta_0 - \cos\theta} \tag{3.22}$$

The leading edge velocity from Theodorsen's theory may be derived from eqn. 3.1.

$$q_{LE} = \sqrt{\frac{2}{r}} \left(C(k) \left(u\alpha - \dot{h} - \dot{\alpha} c \left(a - \frac{3}{4} \right) \right) - \frac{\dot{\alpha} c}{4} \right) \tag{3.23}$$

The stagnation point is derived from eqn. 3.4. The chord-wise wake induced velocity is zero owing to the planar wake assumption, and the second-order term $\dot{h}\alpha$ can be neglected for small amplitudes, giving the stagnation point expression

$$x_s = c{A_0}^2 = c \left(C(k) \left(\alpha - \frac{\dot{h}}{u} - \frac{\dot{\alpha} c}{u} \left(a - \frac{3}{4} \right) \right) - \frac{\dot{\alpha} c}{4u} \right)^2 \tag{3.24}$$

The composite pressure distribution for Theodorsen's theory is obtained from eqn. 2.28, with the Fourier coefficients given by eqns. 3.20.

For very low reduced frequencies, we note that $k \approx 0$, $C(k) = 1 + 0i$, and all the results for Theodorsen's method derived above become the same as those for quasi-steady theory with small-angle approximations applied.

3.2. *Verification with Computational Fluid Dynamics*

Numerical verification of the results derived above is carried out using the open-source CFD toolbox OpenFOAM. A body-fitted computational mesh is moved in accordance with prescribed rate laws, and the time-dependent governing equations are solved using a finite volume method. A second-order backward implicit scheme is adopted to discretise the transient terms, and second-order Gaussian integration schemes with linear interpolation for the face-centred values of the variables are used for the gradient, divergence and Laplacian terms. The pressure implicit with splitting of operators (PISO) algorithm is employed to achieve pressure-velocity coupling. This setup has been previously used to implement the incompressible Navier-Stokes equations and study limit-cycle oscillation of a 2-degree-of-freedom aerofoil (Wang *et al.* 2018), and leading-edge vortex shedding on finite wings of different aspect ratios (Bird & Ramesh 2018; Bird *et al.* 2019). In this research, the incompressible Euler equations are implemented in order to best match the conditions under which the theory (potential flow) is derived. This is done by considering laminar flow, with viscosity set to zero, and using a slip boundary condition for the moving aerodynamic surface. A NACA0004 section is considered, again in order to best match the thin-aerofoil assumption in theory. An O-mesh is constructed with 360 cells around the aerofoil (with a very fine resolution near the leading edge to accurately resolve the stagnation point location), 252 cells in the wall-normal direction, and with the farfield extending to 25 chord lengths in all directions from the aerofoil. The stagnation point from CFD is identified as the location on the aerofoil which is at maximum (stagnation) pressure.

3.2.1. *Harmonic plunge and pitch*

The expressions for stagnation point and composite pressure difference in Theodorsen's theory derived earlier are validated against Euler CFD for a NACA0004 aerofoil using small-amplitude, harmonic, pitch and plunge kinematics.

First, a sine function of plunge is considered by taking the imaginary part of the complex motion, $h = h_0 e^{i\omega t}$, with $h_0/c = 0.03$ and $k = 1.0$. Figure 3 shows the lift

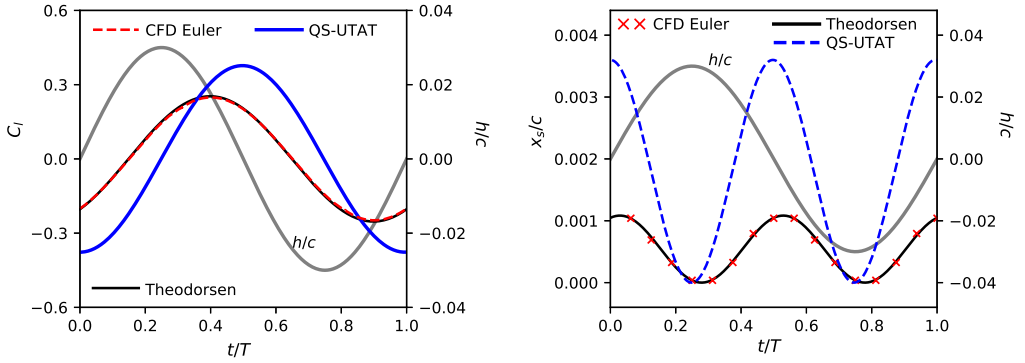

FIGURE 3. Lift coefficient (left) and stagnation-point location (right) comparison for a pure plunge case with $h_0 = 0.03$ and $k = 1.0$. Plunge history is shown on the right axis of each plot.

coefficient and stagnation location variations from CFD, Theodorsen's theory and quasi-steady theory for this case. The right axis in both plots show the plunge variation over the cycle. The quasi-steady result is shown along with Theodorsen's to demonstrate the influence of the wake on the lift and stagnation point locations. An excellent match between the predictions from Theodorsen and CFD is observed. We note that the lift coefficient is not affected by resolution of the leading-edge singularity and is only shown to illustrate the effect of unsteadiness (between quasi-steady and Theodorsen's theory) and to provide a reference for the pressure distributions shown later.

The leading-edge radius is $\approx 0.0018c$ for a NACA0004 aerofoil. Pressure difference coefficient over the aerofoil chord from CFD is compared against the inner, outer and composite solutions from Theodorsen in figure 4. Equally spaced time instants $t/T = 0.25$ and 0.5 are shown, noting that the curves for $t/T = 0.75$ and 1.0 are the exact negatives of these owing to the symmetry in this case. The insets in these plots show the zoomed-in pressure difference near the leading edge. We observe that the composite solution is the same as the inner solution very close to the leading edge, and merges into the outer solution aft of the leading-edge radius region. The outer solution matches best with the CFD result after about $0.5\%c$, but goes to infinity as the leading edge is approached. The composite solution introduces a small error but correctly goes to zero at the leading-edge, following the same trend as CFD. The composite solution also correctly predicts the local maxima/minima which is reflected in the accurate prediction of stagnation point location in fig. 3.

Next, a sine pitch case is considered using the imaginary part of $\alpha = \alpha_0 e^{i\omega t}$ with $\alpha_0 = 3^o$, $k = 0.4$ and pitch-axis at the leading edge. Figure 5 shows the lift coefficient and stagnation location variations from CFD, Theodorsen's theory and quasi-steady theory. Excellent agreement between CFD and Theodorsen's theory is observed. Pressure difference coefficient over the aerofoil chord from CFD is compared against the inner, outer and composite solutions from Theodorsen in figure 6, again only for the first half of the cycle owing to symmetry. Similar trends as for the plunge case are seen. The difference between CFD and the composite solution is most visible for $t/T = 0.5$ (and 1.0) where the value of A_0 is close to zero.

3.2.2. *Ramp-up pitch manoeuvre*

Next, the general unsteady thin-aerofoil theory with leading-edge correction is validated by considering a non-harmonic pitch manoeuvre. The pitch variation is defined

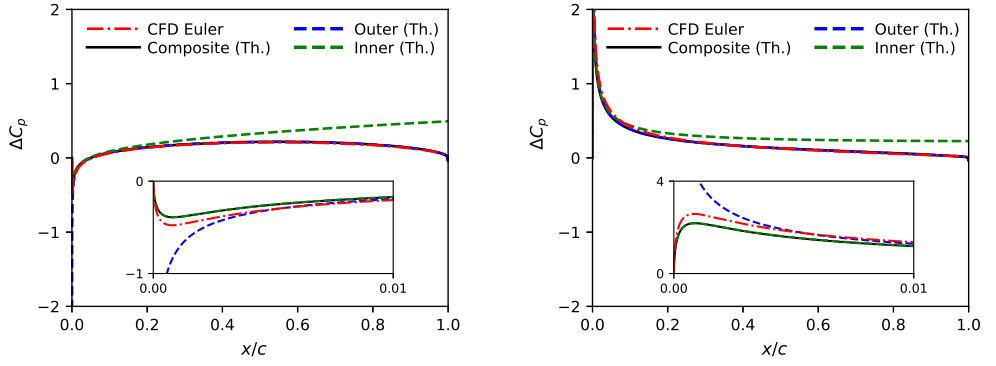

FIGURE 4. Pressure difference coefficient over the aerofoil chord for the pure plunge case from CFD and inner, outer and composite solutions from Theodorsen, at $t/T = 0.25$ (left) and 0.5 (right). Insets show zoomed-in values at leading edge up to 1% of chord.

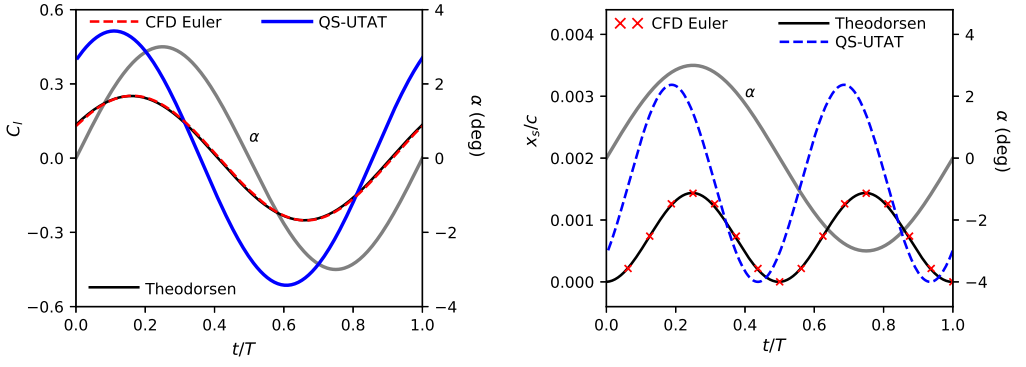

FIGURE 5. Lift coefficient (left) and stagnation-point location (right) comparison for a pure pitch case with $\alpha_0 = 3^o$ and $k = 0.4$. Pitch history is shown on the right axis of each plot.

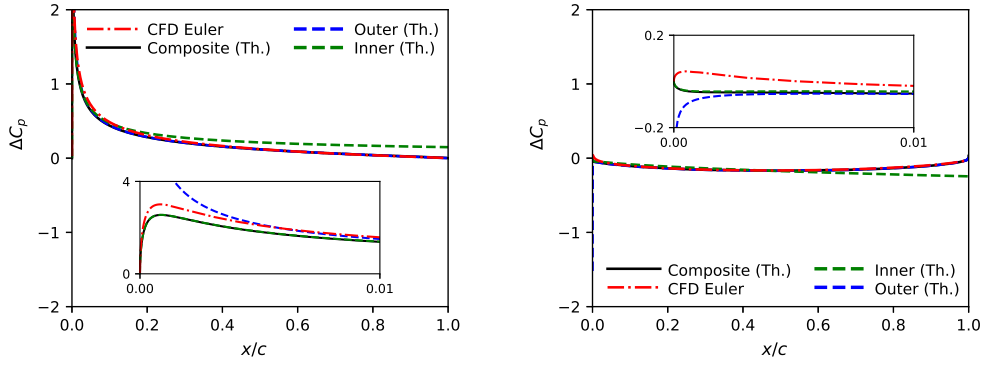

FIGURE 6. Pressure difference coefficient over the aerofoil chord for the pure pitch case from CFD and inner, outer and composite solutions from Theodorsen, at $t/T = 0.25$ (left) and 0.5 (right). Insets show zoomed-in pressure difference at leading edge up to 1% of chord.

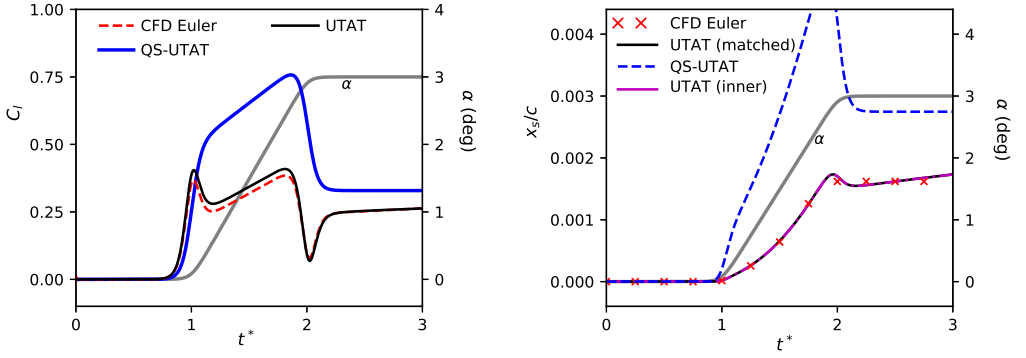

FIGURE 7. Lift coefficient (left) and stagnation-point location (right) comparison for the ramp-up manoeuvre. Pitch history is shown on the right axis of each plot.

using the Eldredge function which produces a ramp motion with smoothed corner (Eldredge *et al.* 2009; Granlund *et al.* 2013).

$$\alpha = \frac{K}{a_s}\left[\frac{\cosh(a_s(t^* - t_1^*))}{\cosh(a_s(t^* - t_2^*))}\right] + \frac{\alpha_0}{2} \tag{3.25}$$

where a_s is a smoothing parameter defined as:

$$a_s = \frac{\pi^2 K}{2\alpha_0(1-\sigma)} \tag{3.26}$$

and,

$$t_2^* = t_1^* + \frac{\alpha_0}{2K} \tag{3.27}$$

Here, t_1^* denotes the nondimensional time ($t^* = tu/c$) at start of ramp, taken as 1.0. The parameter σ is a nondimensional measure of smoothing, set to 0.8. α_0 is the amplitude of the ramp, equal to 3 deg. K is the reduced frequency of pitch taken as 0.026 so that the nondimensional ramp duration is approximately equal to 1.0. Pitch-axis is located at the leading edge. The pitch history is shown on the right axis of the plots in fig. 7. In this figure, lift coefficient and stagnation-point location from quasi-steady theory, unsteady thin-aerofoil theory and Euler CFD are compared. In this case, the stagnation-point $x-$location is nearly equal to the leading-edge radius of the NACA0004 aerofoil (0.0018) during the top of the ramp. Despite this, the stagnation points from unsteady thin-aerofoil theory calculated from both the inner solution and the full matched solution shown in fig. 7 are seen to be identical. The large difference between the quasi-steady and unsteady prediction demonstrates the importance of wake-induced velocity for this case. Unlike in the previous examples, the C_l from unsteady theory is seen to differ mildly from CFD during the ramp. There is still a very good agreement in stagnation point prediction.

Pressure difference coefficient over the aerofoil chord from CFD and the inner, outer and composite solutions from UTAT are compared in figure 8. These plots show differences between CFD and UTAT near the trailing-edge (that results in the difference in lift coefficient observed earlier) which could be related to deviations from the Kutta condition imposed in UTAT (Xia & Mohseni 2017). Apart from this, there is very good agreement between the two methods, including near the leading edge.

While the validations performed above were for small amplitude kinematics, the derivations for unsteady thin-aerofoil theory are valid for arbitrarily large amplitudes

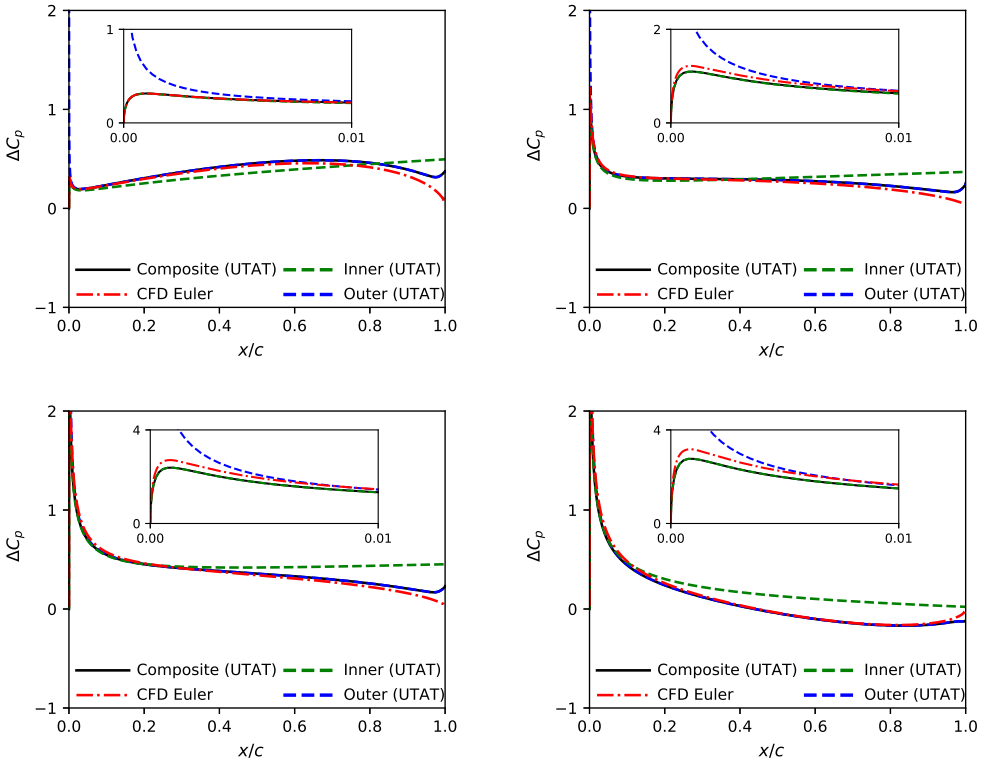

FIGURE 8. Pressure difference coefficient over the aerofoil chord for the ramp-up case from CFD and inner, outer and composite solutions from UTAT, at $t^* = 1.0$ (top left), 1.25 (top right), 1.75 (bottom left) and 2.0 (bottom right). Insets show zoomed-in pressure difference at leading edge up to 1% of chord.

and nonplanar wakes. However, for physically meaningful results, the theory must be supplemented with models/corrections to account for flow separation and vortex shedding that would occur for such kinematics, as in Ramesh *et al.* (2014) and Narsipur *et al.* (2018), for example. CFD validation must also be performed with the full Navier-Stokes equations accounting for viscous effects.

4. Conclusions

The leading-edge singularity in unsteady thin-aerofoil theory is resolved by considering an inner solution of unsteady flow past a parabola and applying the principle of MAE. Composite expressions for pressure difference and velocity distributions, that are uniformly valid over the entire aerofoil are derived. The expression for velocity in the vicinity of the leading edge is seen to be of a similar form to the steady equivalent, with A_0 playing the role of an effective unsteady angle of attack that consists of contributions from the geometric angle of attack, aerofoil camber, plunge velocity and induced velocities by wake vorticity.

The velocity/suction at the leading edge and location of the stagnation point which are quantities of practical interest, are derived from the composite solution. These quantities are functions of the A_0 term in the unsteady vorticity distribution. Closed form expressions for these quantities in the special case of an aerofoil undergoing small-

amplitude harmonic oscillations in pitch and plunge are also obtained using Theodorsen's function (by deriving the full equivalence between Theodorsen's theory and unsteady thin-aerofoil theory), adding to the classical literature in unsteady aerodynamics. All results and expressions presented are comprehensively validated against high-fidelity numerical simulations.

In addition to the expressions derived for pressure difference, surface velocity and stagnation point location, this research paves the way for investigating boundary-layer properties in unsteady problems, and for developing simple criteria for unsteady flow separation analogous to the Stratford criterion in steady flows.

Acknowledgements

The author gratefully acknowledges the support of the UK Engineering and Physical Sciences Research Council (EPSRC) through grant EP/R008035. CFD results were obtained using the ARCHIE-WeST High Performance Computer (www.archie-west.ac.uk) based at the University of Strathclyde. The three anonymous reviewers are thanked for their critical reading of the manuscript and for suggesting substantial improvements.

Declaration of Interests. None.

REFERENCES

Bird, H. J. A., Otomo, S., Ramesh, K. & Viola, I. M. 2019 A geometrically non-linear time-domain unsteady lifting-line theory. AIAA Paper 2019–1377.

Bird, H. J. A. & Ramesh, K. 2018 Theoretical and computational studies of a rectangular finite wing oscillating in pitch and heave. *Proceedings of the 6th. European Conference on Computational Mechanics (ECCM 6) and the 7th. European Conference on Computational Fluid Dynamics (ECFD 7)* pp. 3944–3955.

Darakananda, D. & Eldredge, J. D. 2019 A versatile taxonomy of low-dimensional vortex models for unsteady aerodynamics. *Journal of Fluid Mechanics* **858**, 917–948.

Deparday, J. & Mulleners, K. 2018 Critical evolution of leading edge suction during dynamic stall. *Journal of Physics: Conference Series* **1037** (2), 022017.

Deparday, J. & Mulleners, K. 2019 Modeling the interplay between the shear layer and leading edge suction during dynamic stall. *Physics of Fluids* **31** (10), 107104.

Drela, M. 1989 Xfoil: An analysis and design system for low reynolds number airfoils. In *Low Reynolds number aerodynamics*, pp. 1–12. Springer.

van Dyke, M. 1956 Second-order subsonic airfoil theory including edge effects. NASA TR 1274.

van Dyke, M. 1964 *Perturbation methods in fluid mechanics*, , vol. 136. Academic press New York.

Eldredge, J. D. & Jones, A. R. 2019 Leading-edge vortices: mechanics and modeling. *Annual Review of Fluid Mechanics* **51**, 75–104.

Eldredge, J. D., Wang, C. & Ol, M. V. 2009 A computational study of a canonical pitch-up, pitch-down wing maneuver. AIAA Paper 2009-3687.

Epps, B. P. & Roesler, B. T. 2018 Vortex sheet strength in the sears, küssner, theodorsen, and wagner aerodynamics problems. *AIAA Journal* **56** (3), 889–904.

Garrick, I. E. 1937 Propulsion of a flapping and oscillating airfoil. NACA Rept. 567.

Granlund, K., Ol, M. V. & Bernal, L. P. 2013 Unsteady pitching flat plates. *Journal of Fluid Mechanics* **733** (1), R5.

Hirato, Y., Shen, M., Gopalarathnam, A. & Edwards, J. R. 2019 Vortex-sheet representation of leading-edge vortex shedding from finite wings. *Journal of Aircraft* pp. 1–15.

James, E. C. 1983 Leading edge separation criterion for an oscillating airfoil. DTIC document AD-P004 175.

von Kármán, T. & Burgers, J. M. 1963 *General Aerodynamic Theory - Perfect Fluids*, , vol. 2 of Aerodynamic theory: a general review of progress. Durand, W. F. , Dover Publications.

Katz, J. & Plotkin, A. 2000 *Low-Speed Aerodynamics*. Cambridge Aerospace Series.

Leishman, J. G. 2002 *Principles of Helicopter Aerodynamics*. Cambridge Aerospace Series.

Lighthill, M. J. 1951 A new approach to thin aerofoil theory. *The Aeronautical Quarterly* **3** (3), 193–210.

Morris, W. J. & Rusak, Z. 2013 Stall onset on aerofoils at low to moderately high reynolds number flows. *Journal of Fluid Mechanics* **733**, 439–472.

Narsipur, S., Gopalarathnam, A. & Edwards, J. R. 2018 Low-order model for prediction of trailing-edge separation in unsteady flow. *AIAA Journal* **57** (1), 191–207.

Ramesh, K., Gopalarathnam, A., Edwards, J. R., Ol, M. V. & Granlund, K. 2013 An unsteady airfoil theory applied to pitching motions validated against experiment and computation. *Theoretical and Computational Fluid Dynamics* **27** (6), 843–864.

Ramesh, K., Gopalarathnam, A., Granlund, K., Ol, M. V. & Edwards, J. R. 2014 Discrete-vortex method with novel shedding criterion for unsteady airfoil flows with intermittent leading-edge vortex shedding. *Journal of Fluid Mechanics* **751**, 500–538.

Ramesh, K., Granlund, K., Ol, M. V., Gopalarathnam, A. & Edwards, J. R. 2018 Leading-edge flow criticality as a governing factor in leading-edge vortex initiation in unsteady airfoil flows. *Theoretical and Computational Fluid Dynamics* **32** (2), 109–136.

Ramesh, K., Monteiro, T. P., Silvestre, F. J., Bernardo, A., Neto, G., Versiani, S., de Souza, T. & Gil Annes da Silva, R. 2017 Experimental and numerical investigation of post-flutter limit cycle oscillations on a cantilevered flat plate. International Forum on Aeroelasticity and Structural Dynamics, Como, Italy.

Ramesh, K., Murua, J. & Gopalarathnam, A. 2015 Limit-cycle oscillations in unsteady flows dominated by intermittent leading-edge vortex shedding. *Journal of Fluids and Structures* **55**, 84–105.

Rusak, Z. 1993 Transonic flow around the leading edge of a thin airfoil with a parabolic nose. *Journal of Fluid Mechanics* **248**, 1–26.

Rusak, Z. 1994 Subsonic flow around the leading edge of a thin aerofoil with a parabolic nose. *European Journal of Applied Mathematics* **5** (3), 283–311.

Saini, A. & Gopalarathnam, A. 2018 Leading-edge flow sensing for aerodynamic parameter estimation. *AIAA Journal* pp. 1–13.

Stratford, B. S. 1959 The prediction of separation of the turbulent boundary layer. *Journal of Fluid Mechanics* **5** (1), 1–16.

Suryakumar, V. S., Babbar, Y., Strganac, T. W. & Mangalam, A. S. 2016 Unsteady aerodynamic model based on the leading-edge stagnation point. *Journal of Aircraft* **53** (6), 1626–1637.

Theodorsen, T. 1935 General theory of aerodynamic instability and the mechanism of flutter. NACA Rept. 496.

Wang, E., Ramesh, K., Killen, S. & Viola, I. M. 2018 On the nonlinear dynamics of self-sustained limit-cycle oscillations in a flapping-foil energy harvester. *Journal of Fluids and Structures* **83**, 339–357.

Willis, D. J. & Persson, P. 2014 Multiple-fidelity computational framework for the design of efficient flapping wings. *AIAA journal* **52** (12), 2840–2854.

Xia, X. & Mohseni, K. 2017 Unsteady aerodynamics and vortex-sheet formation of a two-dimensional airfoil. *Journal of Fluid Mechanics* **830**, 439–478.